Electronic Supplementary Material (ESI) for Journal of Materials Chemistry C.

Supporting Information

Exploring Thermal Transitions in Anthradithiophene-based Organic Semiconductors to Reveal Structure-Packing Relationships

Shi Li, Sean M. Ryno, & Chad Risko

Department of Chemistry &
Center for Applied Energy Research
University of Kentucky
Lexington, Kentucky 40506 USA

Corresponding author: chad.risko@uky.edu

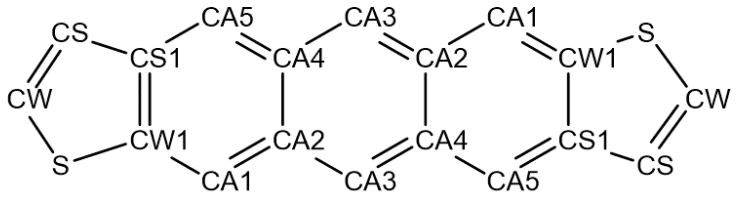

anti ADT

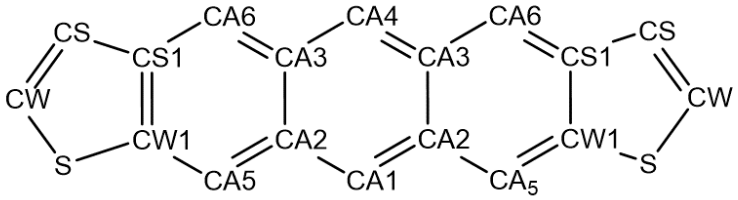

syn ADT

Figure S1. Chemical structures of *anti* and *syn* ADT with atom labels used for the bond and angle analyses.

Table S1. Select bond lengths for *anti* and *syn* ADT as determined by molecular mechanics (MM) energy minimization using the OPLS-AA force field and density functional theory (DFT) optimizations at B3LYP/6-31G(d,p) level. Atom labels are given in Figure S1.

	***anti* ADT**			***syn* ADT**		
Bond #	DFT [Å]	MM [Å]	SD	DFT [Å]	MM [Å]	SD
S-CW	1.761	1.753	0.004	1.761	1.768	0.004
CW-CS	1.353	1.365	0.006	1.353	1.358	0.003
CS-CS1	1.446	1.458	0.006	1.446	1.446	0.000
CS1-CA5	1.379	1.386	0.003	-	-	-
CA4-CA5	1.422	1.424	0.001	-	-	-
CA3-CA4	1.402	1.409	0.004	1.402	1.409	0.004
CA2-CA3	1.400	1.412	0.006	-	-	-
CA1-CA2	1.427	1.427	0.000	1.401	1.418	0.008
CA1-CW1	1.370	1.370	0.000	-	-	-
CW1-S	1.769	1.769	0.000	1.769	1.767	0.001
CW1-CS1	1.444	1.450	0.003	1.444	1.453	0.005
CA2-CA3	1.453	1.451	0.001	1.453	1.462	0.004
CS1-CA6	-	-	-	1.379	1.374	0.002
CA3-CA6	-	-	-	1.423	1.430	0.003
CA5-CW1	-	-	-	1.370	1.385	0.007

Table S2. Select bond angles for *anti* and *syn* ADT determined by molecular mechanics (MM) energy minimization using the OPLS-AA force field and density functional theory (DFT) optimizations at B3LYP/6-31G(d,p) level. Atom labels are given in Figure S1.

Angle	*anti* ADT			*syn* ADT		
	DFT [°]	MM [°]	SD	DFT [°]	MM [°]	SD
S-CW1-CS1	113.893	114.584	0.346	113.887	113.713	0.087
CW1-CS1-CS2	113.228	112.540	0.344	113.224	113.679	0.227
CS1-CS2-CW2	110.476	110.980	0.252	110.477	110.761	0.142
CS2-CW2-S	110.767	111.361	0.297	110.768	111.385	0.309
CW2-S-CW1	90.637	90.536	0.050	90.644	90.460	0.092

Table S3. Unit cell parameters and densities determined from MD simulations using the OPLS-AA force field in comparison to those from the experimental crystal structure reported in ACS Applied Materials & Interfaces 2013, 5, 9670.

	***anti* ADT**			***syn* ADT**		
	MD	CIF	SD	MD	CIF	SD
a [Å]	5.972	5.916	0.028	5.916	5.887	0.014
b [Å]	7.846	7.772	0.037	7.545	7.508	0.018
c [Å]	14.125	13.991	0.067	14.418	14.347	0.035
α [°]	86.600	86.589	0.005	96.160	96.100	0.030
β [°]	78.300	78.271	0.014	94.300	94.300	0.000
γ [°]	86.400	86.424	0.012	89.600	90.400	0.400
Density [g/cm^3]	1.490	1.540	0.025	1.510	1.530	0.010

Table S4. Potential of mean force (PMF) minima center- of-mass (COM) distances and those obtained from the respective crystal structures.

	PMF		Bulk Crystal (nm)
	Minima (nm)	Plateau (nm)	
anti ADT	0.389	1.510	0.474
syn ADT	0.400	1.520	0.488
anti TES ADT	0.404	1.910	0.673
syn TES ADT	0.404	1.910	0.630

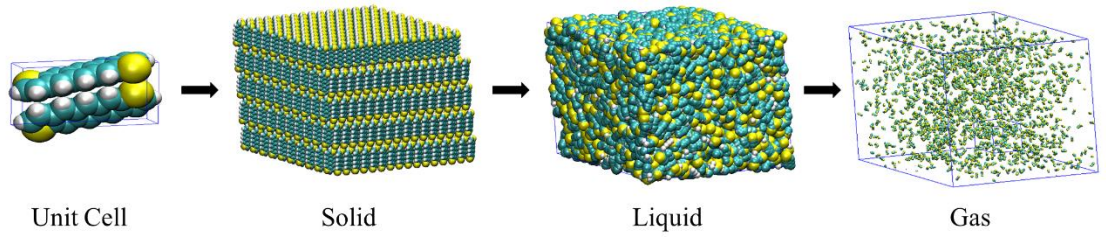

Figure S2. Annealing simulation work protocol.

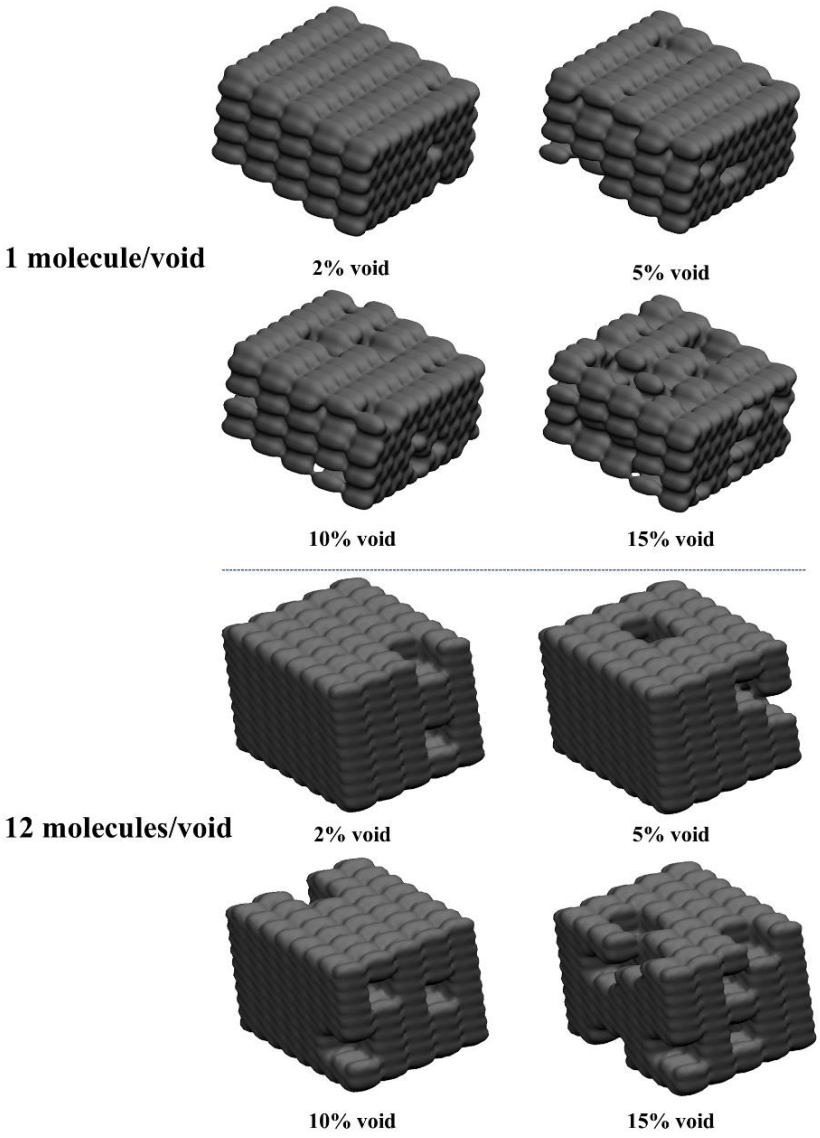

Figure S3. Representations of the void methods implemented. (Top) Each void was created by removing one molecule to create the void. (Bottom) Each void was created by removing a group of 12 molecules to create the void. The void percentage was calculated based on the total number of molecules removed from the bulk crystal.

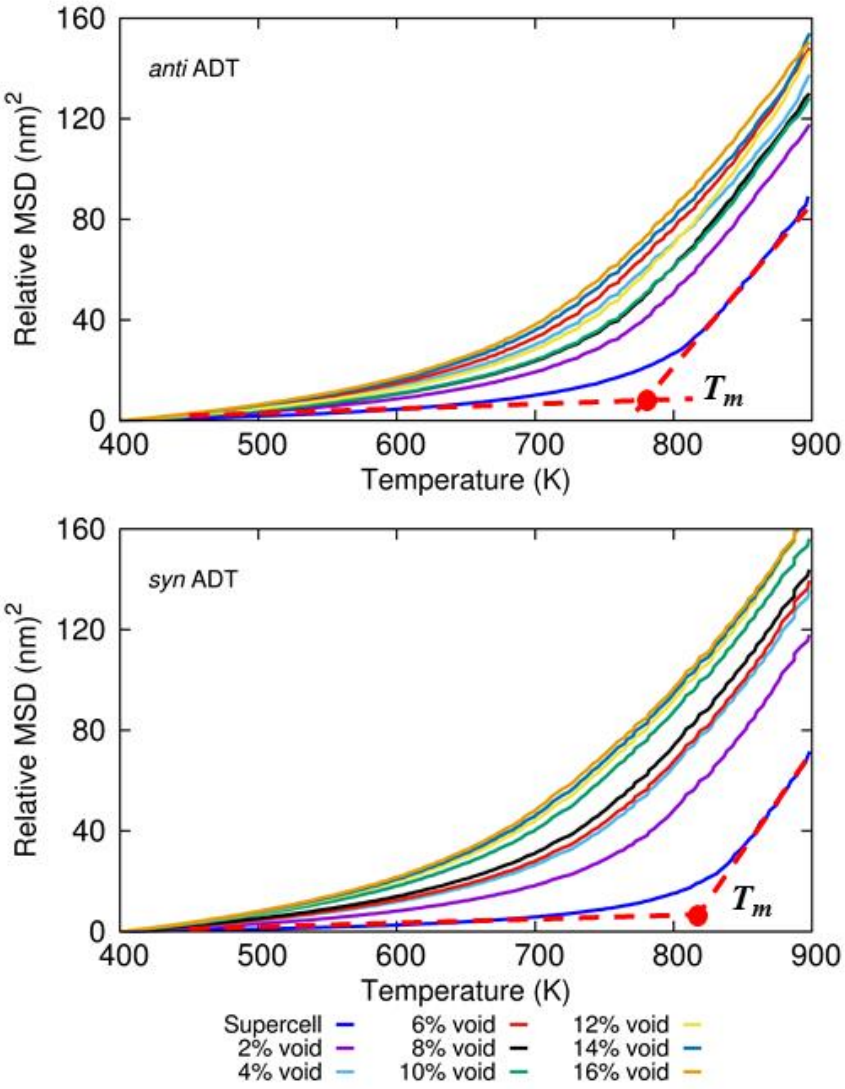

Figure S4. Relative MSD as a function of anneal temperature of the *anti* and *syn* ADT systems with voids of varying percentage. The MSD of the void free supercell for each system is also included. Dashed lines indicate the two linear trend lines of solid and liquid phases, and the intersection T_m is marked for reference; one example is given in each plot.

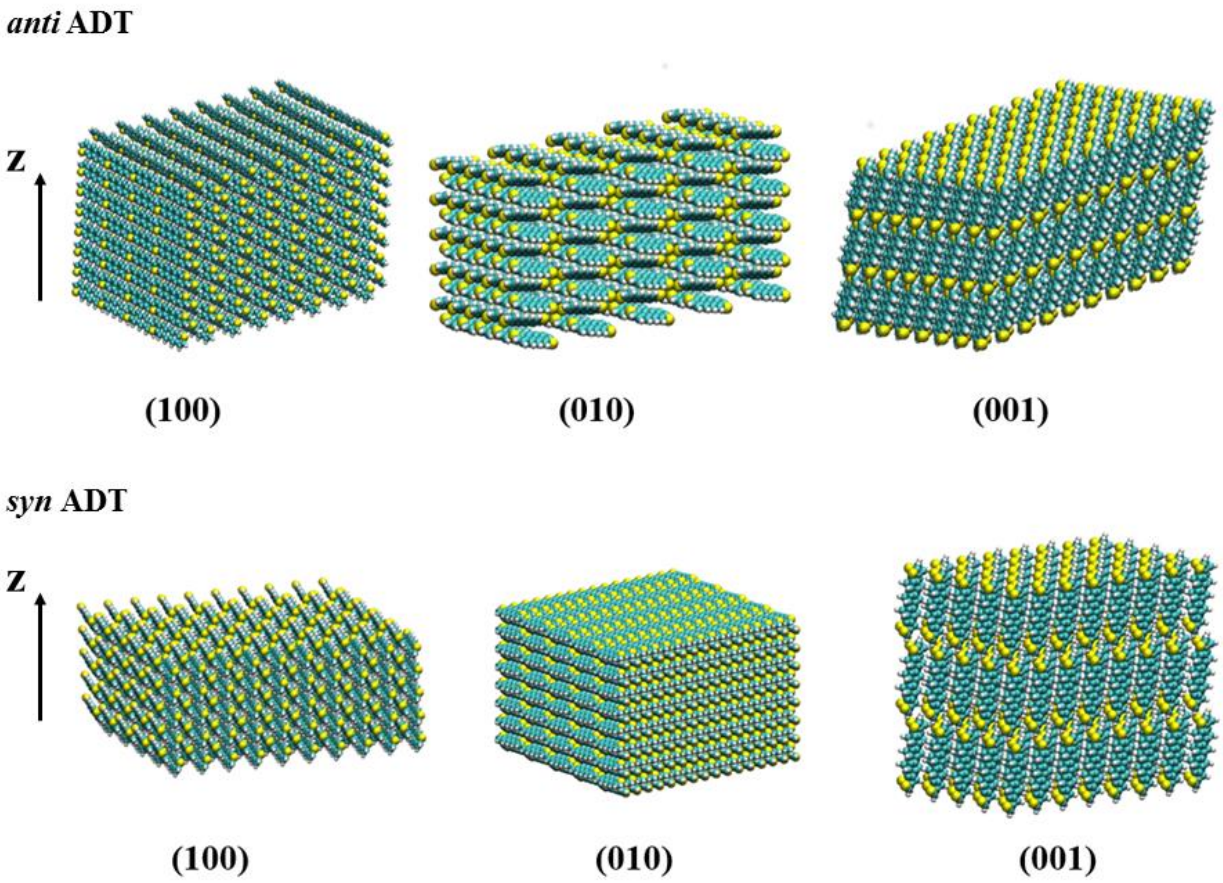

Figure S5. *Anti* (top) and *syn* (bottom) ADT slabs; the vacuum gap is along *z*-direction.

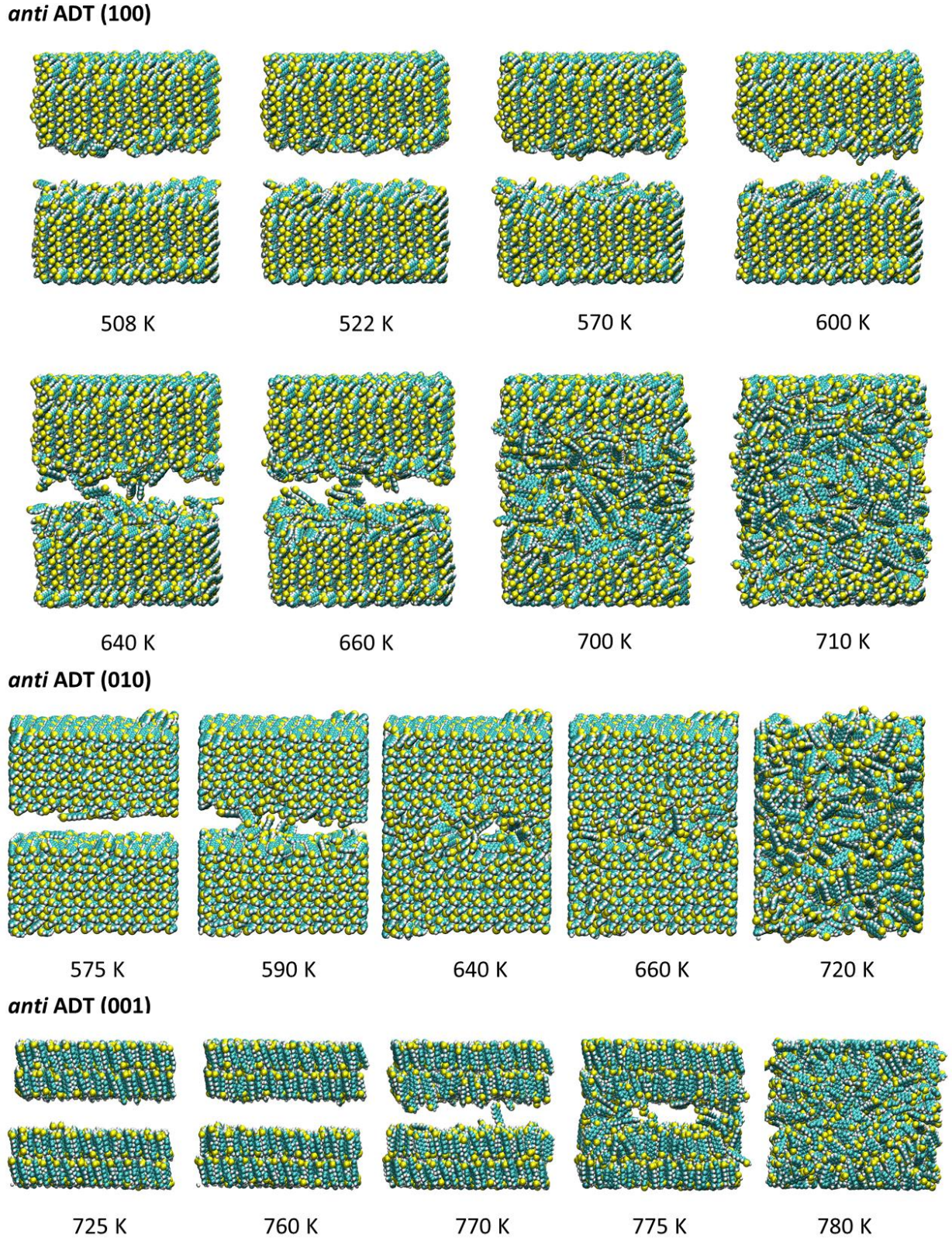

Figure S6. Snapshots of sdifferent *anti* ADT slabs during annealing.

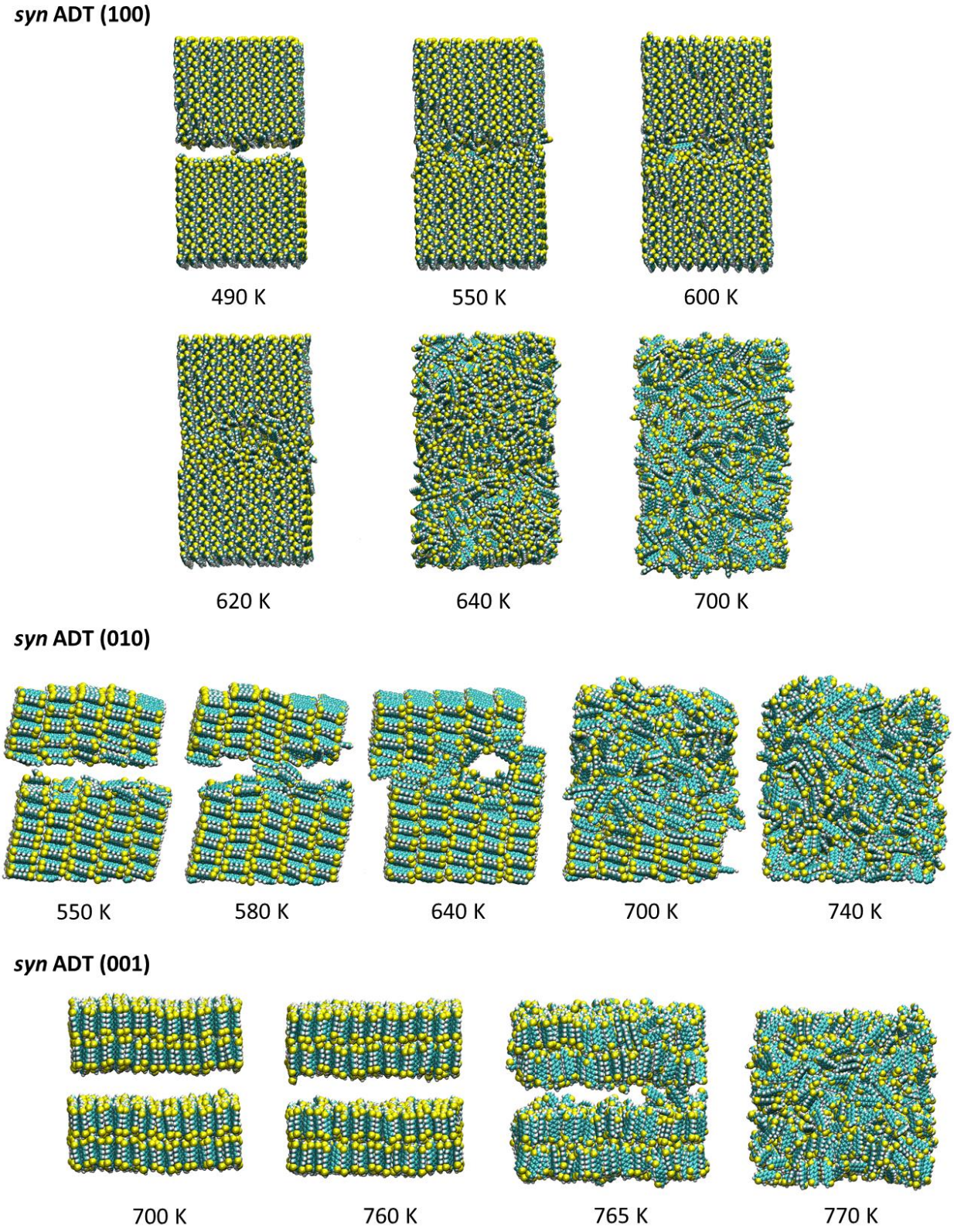

Figure S7. Snapshots of different *syn* ADT slabs during annealing.

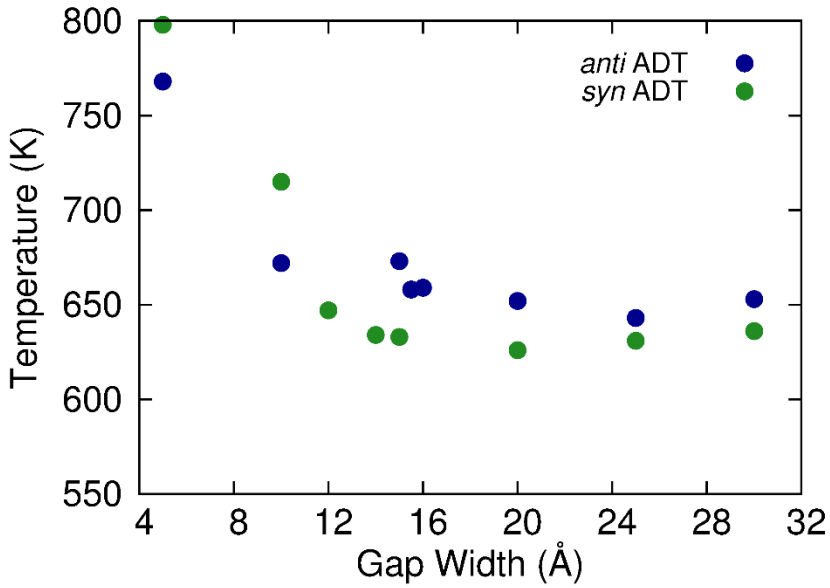

Figure S8. T_m as a function of the (010) gap width for *anti* (blue dot) and *syn* (green dot) ADT.

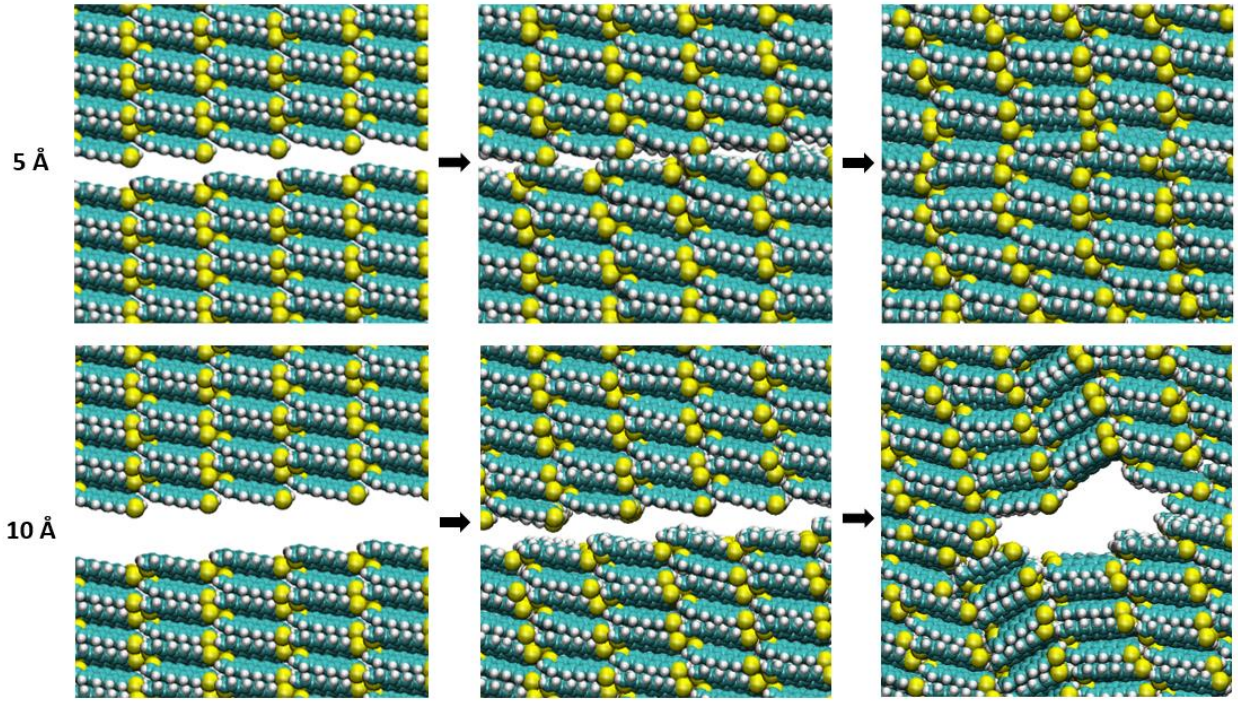

Figure S9. *Anti* ADT with 5 Å and 10 Å vacuum gap along the (010) surface to demonstrate differences in the melting process as a function of vacuum gap width during NVT equilibrium.

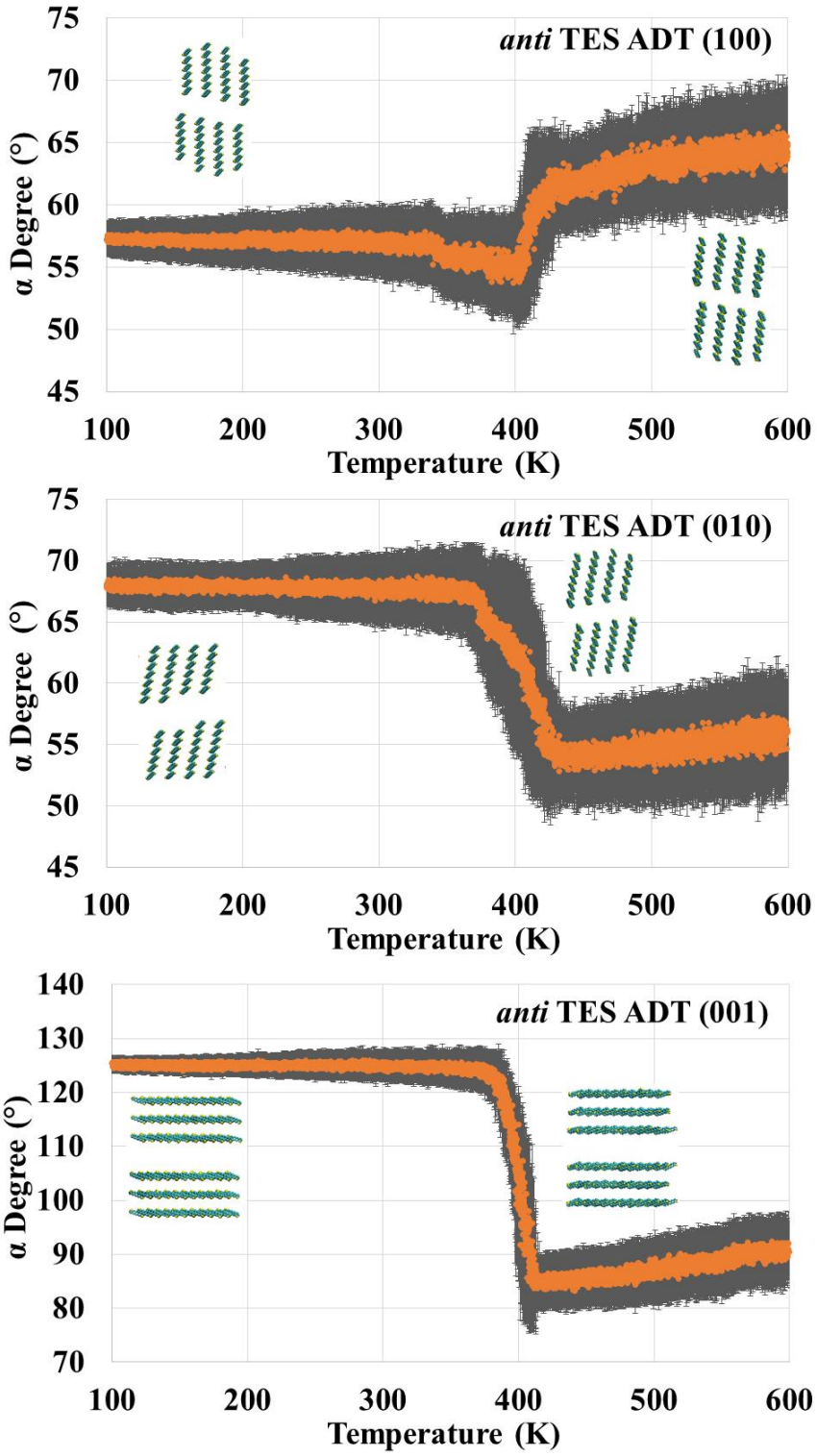

Figure S10. The angle between *anti* TES ADT backbone long-axis vector with respect to the *z*-direction as function of the annealing temperature of different slab systems. The inset snapshots show the backbone directions before and after reorientation.

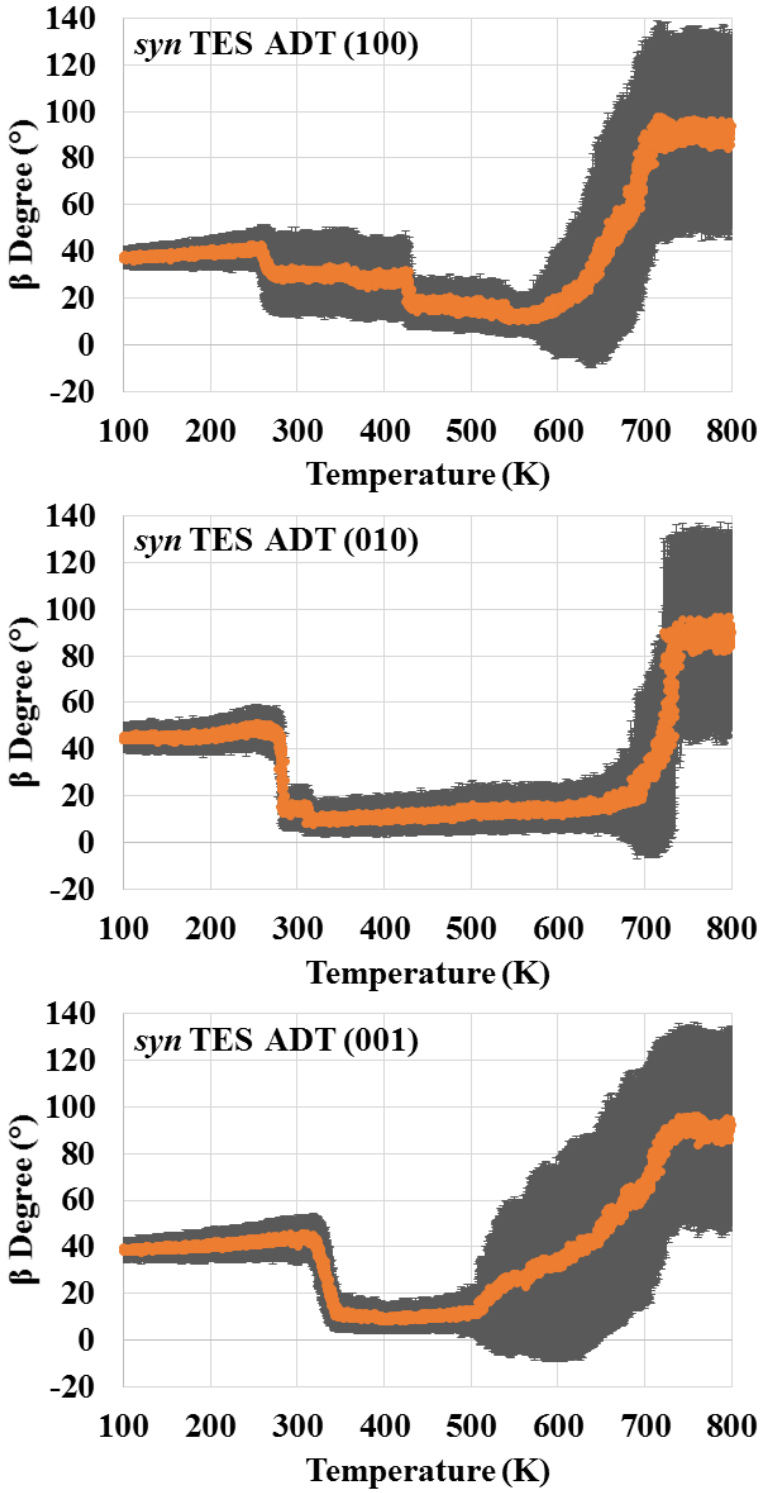

Figure S11. Angle between the two molecular planes in the same unit cell as a function of temperature.

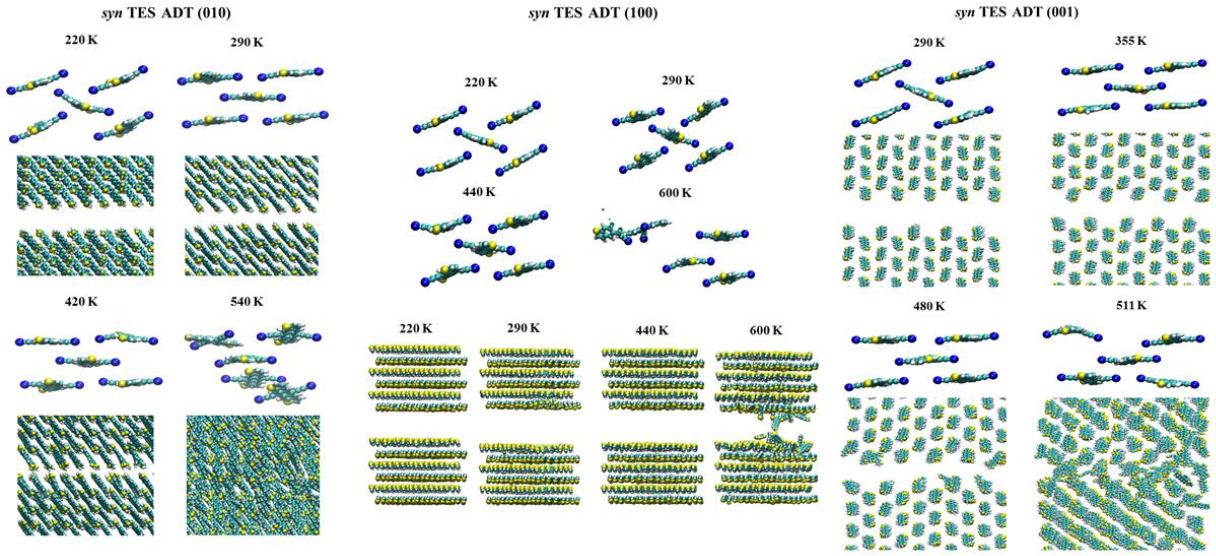

Figure S12. Snapshots of three *syn* TES-ADT slab systems during thermal annealing, showing the molecular reorientation before melting.

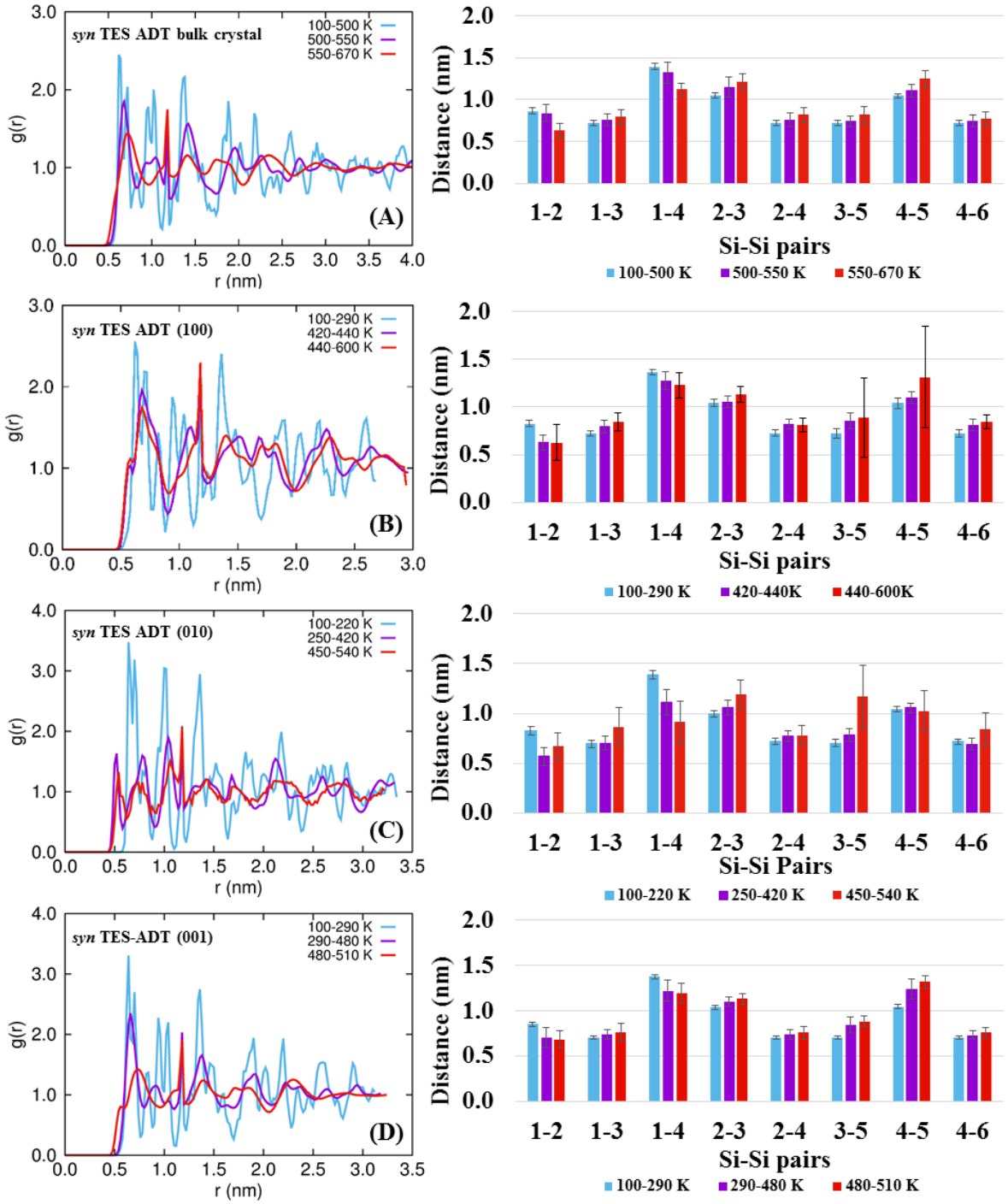

Figure S13. (Left) Radial distribution functions [g(r)] for Si-Si pairs in the *syn* TES ADT bulk crystal and slab systems. (Right) Distances of Si-Si pairs at various stages of the thermal annealing process. The Si numbering is given in Figure 12.